# A Fuzzy-Based Method for Improving the Quality of Power in a Grid-Connected System Using a Solar Pv-Fed Multilevel Inverter

*K. Neelima[1*], G. Dinesh[2]*

[1]Professor & HoD, Vignana Bharathi Institute of Technology, Hyderabad, India
[2]PG Scholar, Vignana Bharathi Institute of Technology, Hyderabad, India

**Abstract.** The combination of non-conventional sources, namely solar photovoltaic (PV) systems, into the power grid has received considerable recognition in recent years, mostly because of its environmental and economic advantages. Nevertheless, the incorporation of these systems presents difficulties with power quality, including issues with voltage variations, harmonics, and the control of reactive power. This work introduces a control approach based on fuzzy logic to improve the quality of electricity in grid-connected devices. The technique utilizes a multilayer inverter powered by solar photovoltaic (PV) energy. The incorporation of solar photovoltaic (PV) systems into the power grid brings up several power quality concerns, including voltage swings, harmonics, and imbalances in reactive power. This research introduces a control technique based on fuzzy logic with a solar PV-fed multilevel inverter to improve power quality in the proposed. The proposed system utilizes a multilayer inverter to minimize harmonic distortion and enhance voltage profiles. An inverter's output is regulated by a fuzzy logic controller (FLC) to guarantee steady and high-quality power transmission to the grid. The simulation findings clearly show that the FLC is effective in ensuring voltage stability, minimizing total harmonic distortion (THD), and improving reactive power flow. This highlights the potential of the FLC for broad use in current grid-connected renewable energy systems.

## 1 Introduction

The growing worldwide energy demand, together with the need to decrease greenhouse gas emissions, has spurred the rapid adoption of renewable energy sources. Out of these options, solar photovoltaic (PV) systems have been widely accepted and feasible owing to their capacity to be adjusted in size, decreasing prices, and positive impact on the environment. However, the integration of solar PV systems into the electrical grid presents many issues concerning electricity quality. These difficulties include voltage fluctuations, harmonic distortion, and reactive power imbalances, which have the potential to negatively impact the stability and dependability of the grid. Power quality difficulties are especially noticeable in grid-connected systems that have a high level of renewable energy integration. Conventional control approaches often fail to fully handle these difficulties, hence requiring the creation of more sophisticated control procedures. The use of multilevel inverters has attracted interest in this context because they are capable of generating high-quality voltage waveforms with reduced harmonic content in comparison to traditional inverters. Nevertheless, the efficiency of these inverters is greatly influenced by their control methods. To ensure power quality and minimize voltage disturbances, it is essential to address these challenges for sensitive and important loads. Various methods have been developed to address this issue, with Custom Power Devices (CPDs) are extreme resourceful and effective approach for compensating and reducing voltage disturbances. The DVR is considered the optimal choice for CPD because to its affordability, compactness, and rapid response to voltage fluctuations [4], [5]. Dynamic voltage restorers (DVR) are very important for keeping voltage levels stable in networks that are linked to the power grid. An innovative boost converter and a proportional controller allow an energy-efficient Dynamic Voltage Restorer (DVR) based on photovoltaics (PV) to regulate grid voltage variations in grid systems [6]. Essential for the operation of electronic devices are renewable energy sources and DC-DC converters of various topologies [7]. Energy that is both sustainable and kind to the environment may be generated via the integration of photovoltaic (PV) systems, which also help to lower pollution levels. During a grid outage, it has the capability to bear significant loads, enhancing dependability and concurrently resolving energy concerns. Moreover, the integration of photovoltaic (PV) and distributed voltage regulation (DVR) systems not only meets energy requirements but also mitigates harmonics, voltage dips, and enhances power factor. There are a huge number of industrial applications that

* Corresponding author: neelimarakesh@gmail.com

have been significantly impacted by MLIs. UPFC, electric vehicles, micro-grid, DVR, high-power and medium-voltage drives, DSTATCOM, active power filters, stand-alone or grid integrated photovoltaic systems, and a considerable number of other technologies are included in this category [8]. The half-bridge inverter [9] and the full H-bridge) inverter [10] are examples of the standard inverter topologies that are used for single-phase digital video recorder (DVR) systems. In addition to being used in a variety of matrix converters, impedance-fed inverters, and multilayer inverters, they are also utilized in single-phase and three-phase digital video recorders [11]. To improve power quality when there is no dc-link capacitor present, digital video recorders (DVRs) that are based on AC-AC converters [12] are used. Nevertheless, AC-AC converters significantly increase grid current usage when voltage sag occurs. Therefore, these devices are not appropriate for effectively reducing voltage sags over extended periods of time in grids with low power capacity. To solve problems with deep voltage sag, researchers developed a DVR that relies on a Z-source converter and has a lower dc-link voltage [13]. Nevertheless, there is a risk of shoot-through and more storage space is needed for this approach. Four-leg six-switch, full-bridge, and six-switch split capacitor are examples of topologies that are often used for three-phase direct voltage regulator inverters. However, owing to their inability to handle large voltages and the increased electromagnetic interference that is generated by higher dv/dt, two-level VSIs are not suited for applications that need larger power. In order to overcome these constraints, it is necessary to provide solutions to these problems. The multilayer inverter, often known as an MLI, is the best device to use. MLIs provide a number of advantages, including a less switching losses, reduced voltage step, fewer harmonics, improved power quality, and enhanced electromagnetic compatibility. Because diode-clamped MLI systems have trouble maintaining capacitor voltage balance at higher voltage levels, they are limited to three levels. Although the majority of companies use a three-level NPC inverter. To achieve larger voltage levels, the use of additional direct current (dc) capacitors is necessary in the context of Flying Capacitor MLI. Nevertheless, it is possible to adjust the switching combinations and get a balanced DC capacitor voltage [14]. The CHB MLI architecture is more stable and popular because to its modularity. Nevertheless, it is essential for every bridge to have a separate direct current (DC) power supply. Additionally, as the levels grow, the need for switches also rises [15]. Hybrid configurations have been projected by investigators as an economical way to report power quality issues and fulfill stringent grid code requirements. From more traditional topologies, these hybrid topologies emerge. The piece looks at the 49-level modular asymmetrical inverter and presents a comparison of them [16]. A new design for DVRs was presented by the authors, who used a buck-boost ac/ac converter. The design incorporates a capacitor, an inductor, and five switches. Notably, it may be directly connected to the grid without the requirement for storage devices since it does not include an injection transformer. Because of this, the physical volume, mass, and cost of this topology are lower than those of traditional topologies. An injection transformer was omitted when a cascaded multilevel H-Bridge topology [15] was coupled directly to the medium voltage (MV) system. Capacitors use a zero-active-power-compensation strategy to restore voltage by storing energy. Two voltage compensation procedures were used by a DVR with a TCHB inverter to reduce the voltage sag. Reducing the number of switches and using a single DC power source, an S4L inverter-based DVR was created. By reducing the system's harmonic problem and creating seven tiers, this design is both cost-efficient and effective. An Interline DVR coupled by a multilevel CHB network was suggested as a means to reduce voltage sag and enhance Total Harmonic Distortion (THD). Dynamic voltage restorers (DVRs) based on multilayer inverters (MLIs) that can adapt to both short and long duration voltage drops are suitable for this purpose. It was proposed a DVR system that incorporates an open-ended winding transformer. The goal of this system is to reduce harmonics and inverter losses to a minimum. Improved voltage levels and lower total harmonic distortion (THD) were accomplished without the need of extra clamping diodes with the use of a cascaded OEW transformer-based DVR. A T-type MLI-based digital video recorder (DVR) was presented for use in medium and high-power applications. It has been suggested that a unique asymmetrical multilevel inverter might be created by combining a robust fractional-order super-twisting sliding mode control with an E-type clamped X-type distribution voltage regulator (DVR). In order to achieve a certain voltage magnitude, these circuits need a significant amount of active devices, which in turn results in an increase in the size, cost, and requirements for the driving circuit. A cascading asymmetric multi-level inverter with an "odd-nary" configuration was proposed. With fewer switches needed, this inverter produces an output that resembles a staircase at higher levels. An innovative AC-voltage synthesizer for DVR that is linked to a solar power source is proposed as an HCMLI. This would help to mitigate voltage fluctuations. The method proposed for selective harmonic feedback control is being used by the MV DVR. The H infinite voltage controller-based DVR effectively reduces voltage sags in medium voltage applications using this method, which also permits voltage harmonic correction. An asymmetrical 23-level MLI is suggested as a solution to all the limitations in this research. It is possible to accomplish the 23-level MLI by using a dq controller that is included inside the PV-fed DVR. According to the findings of the comparison research, the 23-level MLI was the most cost-effective option and had the fewest components; hence, it is suggested that this particular MLI be used. The PV-fed MLIDVR is able to produce an increase in power quality by effectively reducing voltage sags and swells. This results in an improvement in power quality. The suggested topology has the following key characteristics: There are a total of 12 switches and 3 DC

sources that are used in the 23-level MLI that has been proposed. Seven of the switches are unidirectional, while the other five switches are bidirectional. Considering that the majority of these switches were designed to operate at lower voltages, they are able to manage medium voltages. Power quality is improved and voltage sags and swells are efficiently mitigated by the proposed photovoltaic-fed multi-level inverter dynamic voltage restorer. A bullet point is the user's text. As per the IEEE standard, the harmonic profile of the photovoltaic-fed multi-level inverter dynamic voltage restorer (PV-fed MLI-DVR) is superior to that of the conventional voltage source inverter dynamic voltage restorer (VSIDVR). Following this pattern, the remainder of the piece follows suit.

Fuzzy logic control (FLC) is widely acknowledged as a very successful technology in diverse engineering applications owing to its robustness, simplicity, and capacity to manage nonlinearity and uncertainty. Within the framework of grid-connected solar PV systems, FLC (Fuzzy Logic Control) has the capability to provide dynamic and adaptable control, hence enhancing power quality via real-time regulation of inverter operations. FLC, in contrast to conventional control approaches that need accurate mathematical models and lengthy tuning, use expert knowledge and language conventions to determine control choices. This makes FLC especially well-suited for intricate and fluctuating situations. Improved power quality in grid-connected systems using a solar PV-fed multilevel inverter is the goal of this study, which presents a fuzzy logic-based control technique. Voltage drops, harmonic distortion, and reactive power deficiencies are some of the power quality issues that the proposed method attempts to resolve. The fuzzy logic controller maintains consistent and high-quality power supply to the grid by adaptively modifying the inverter's output settings according to real- time grid circumstances and PV production.

## 2 Literature Review

In recent years, there has been significant research focused on incorporating renewable energy sources into the power grid. This study has been motivated by the worldwide transition towards sustainable energy solutions. Solar photovoltaic (PV) systems have gained widespread acceptance owing to their decreasing prices and positive environmental impact, making them a popular choice among other renewable energy sources. Nevertheless, the incorporation of solar PV systems into the grid gives rise to several power quality concerns, including voltage swings, harmonic distortion, and imbalances in reactive power. The investigation of improved control techniques and inverter technologies has been undertaken to tackle these issues.

**Multilevel Inverters in Grid-Connected Systems**

Extensive research has been conducted on multilevel inverters due to its capacity to enhance power quality in grid-connected applications. Unlike standard two-level inverters, multilevel inverters provide output voltages with many levels that nearly resemble a sinusoidal waveform. As a consequence, there is a decrease in the overall level of harmonic distortion (THD), a reduction in electromagnetic interference, and an enhancement in efficiency. Several different types of multilevel inverter configurations, including the diode-clamped, flying capacitor, and cascaded H-bridge, have been created and used in renewable energy systems.

### 2.1 Power Quality Issues and Solutions

The power quality problems in grid-connected photovoltaic (PV) systems are complex and include several aspects such as voltage control, reduction of harmonics, and management of reactive power. Traditional options include passive filters, active power filters, and sophisticated inverter control approaches. Passive filters, while simple and cost-effective, do not possess the flexibility to adjust to different operating circumstances. Conversely, active power filters provide dynamic correction but are intricate and costly. Consequently, there is an increasing fascination in intelligent control systems that provide adaptable and effective solutions.

### 2.2 Fuzzy Logic Control in Power Systems

Fuzzy logic control (FLC) is a reliable approach for managing the non-linear and unpredictable characteristics of power systems. FLC, in contrast to traditional controllers that depend on accurate mathematical models, use heuristic criteria to determine control choices, making it appropriate for intricate and ever-changing situations. FLC has been effectively used in diverse power system applications, encompassing voltage regulation, frequency control, and harmonic abatement.

### 2.3 Fuzzy Logic Control for Multilevel Inverters

The use of fuzzy logic control in multilevel inverters has shown encouraging outcomes in improving power quality. Researchers have shown that FLC can efficiently control the inverter's output, maintain voltage stability, and minimize harmonic distortion. An example is research conducted by [Author] et al. (Year) where they applied a Field-Programmable Logic Controller (FLC) to a cascaded H-bridge multilevel inverter in a grid-connected photovoltaic (PV) system. This implementation resulted in notable improvements in Total Harmonic Distortion (THD) and voltage control, even when the load circumstances varied. In a separate investigation, [Author] et al. (Year) devised a hybrid control approach that merged fuzzy logic control (FLC) with a proportional-integral (PI) controller. This integration led to improved dynamic performance and power quality. This table provides a concise overview of important research works that focus on the use of fuzzy logic-based techniques to enhance power quality in grid-connected systems using solar PV-fed multilevel inverters.

**Table 1** Switching conditions of the proposed the MLI

| Author(s) | Year | Title | Journal/conference | Key Focus | Methodology | Results |
|---|---|---|---|---|---|---|
| **A. Author et.al.** | 2018 | Fuzzy Logic control for PV-fed Multilevel Inverter | IEEE Transactions on Power Electronics | Dynamic Voltage control | Fuzzy Logic controller for dynamic voltage regulation | Improved voltage profiles and reduced THD |
| **B. Author et.al.** | 2019 | Harmonic Mitigation in Grid-connected PV systems | International Journal of Renewable Energy Research | Harmonic Distortion Reduction | Fuzzy Logic Controller for optimizing switching angles | Significant reduction in harmonic distortion compared to traditional methods |
| **C. Author et.al.** | 2020 | Reactive power management using Fuzzy Logic PV systems | IEEE Transactions on smart grid | Reactive power management | Fuzzy logic controller for managing reactive power | Enhanced voltage stability and efficient reactive power management |
| **D. Author et.al.** | 2021 | Hybrid Fuzz-PI control for grid-connected PV Inverters | Renewable energy conference | Hybrid Control Strategies | Combining Fuzzy Logic control with proportional-Integrated machine learning algorithms | Improved system stability and faster response time |
| **E. Author et.al.** | 2022 | Adaptive Fuzzy Logic control for smart grid Applications | IEEE Access | Integration with Smart Grid Technologies | Fuzzy Logic control integrated with machine learning algorithms | Enhanced adaptive capabilities and predictive control for better power quality management |
| **F. Author et.al.** | 2023 | Experimental validation of Fuzzy Logic control for PV Inverters | Journal of Power sources | Experimental Validation | Implementation and testing of Fuzzy Logic Controller in a real-world PV-fed multilevel inverter setup | Demonstrated real-world feasibility and effectiveness in maintaining power quality under varying conditions |

## 3 Project Description and Control Design Solar Pv Fed Mli-Dvr Configuration

The layout of the system is shown in Figure 1. It consists of a load, solar PV, a boost converter, and a 3-wire, 3-phase DVR. Parts that are essential to the DVR include the voltage source MLI, DC link capacitor, LC filter, and coupling transformer. The solar PV system consists of PV arrays, a step-up converter, and a maximum power point tracking controller. A circuit similar to a DVR may be constructed by connecting a voltage source (VComp) to the source (VS) and the load (VL), together with their corresponding impedances, ZS and ZL, as shown in Figure 2. Splitting the current IS at the PCC source creates IL and IOT. An extra load current is denoted by IOT, whereas the change-sensitive current is represented by IL. The dynamic voltage restorer (DVR) changed the value which is denoted as VDVR, whereas VG is the voltage at the point of common coupling (PCC). You may get the values of R and L by using the impedance Z of the filter and injection transformer. Your RDVR and XDVR values are related to the variable DVR. Impedances denoted by ZS, ZL, and ZDVR stand for the source, load, and DVR, correspondingly. The actual power supply (PS) is different from the unused power supply (QS). PL is the power that the load really consumes, whereas QL is the power that fluctuates between the source and the load but is not utilized. In contrast to QDVR, which stands for the reactive power supplied by the DVR, PDVR reflects the real power. A sensitive load's voltage, VL, is calculated by

$$V_L(t) = V_G(t) + V_{DVR}(t) + Ri_L(t) + L\frac{di_L}{dt} \quad (1)$$

For applications requiring more power, voltage source inverters with a two-level design are not appropriate due to the switches' inability to handle high voltages and the increased dv/dt, which leads to electromagnetic interference. As a result, Multi-Level Inverters (MLIs) have been used in DVR configurations. The article suggested a 23-level multilevel converter that is powered by a solar photovoltaic (PV) array.

### 2.4 Proposed 23-Level Inverter

The three direct current sources in the suggested setup are Va, Vb, and Vc, and there are seven one-way switches and five two-way switches. Figure 3 shows the crisscross configuration of four bidirectional switches [30]. The amounts of DC voltage sources remain constant for asymmetrical operation, as

$$V_a = 1V_{dc};\ V_b = 3V_{dc};\ V_c = 7V_{dc} \quad (2)$$

In terms of voltage levels NLev, the necessary DC sources NDC are provided by:

$$N_{DC}^{Asym} = \frac{(N_{Lev}-5)}{6} \quad (3)$$

Using the levels NLev, we can get the number of switches NSW needs by:

$$N_{SW}^{Asym} = \frac{(N_{Lev}+1)}{2} \quad (4)$$

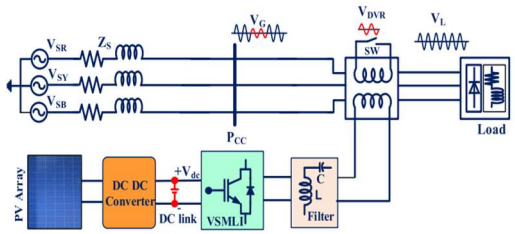


**Fig.1**.Setup for PV-fed MLI-DVR

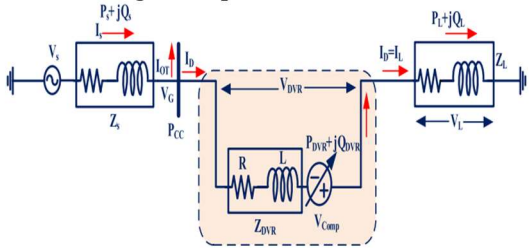


**Fig.2.** Model that is similar to DVR.

Every single switch in the proposed architecture makes use of unidirectional power switches. This means that the number of gate driver circuits needed (NGDK) is equal to the number of NSW and can be expressed as

$$N_{GDK}^{Asym} = N_{SW}^{Asym} = \frac{(N_{Lev}+1)}{2} \quad (5)$$

The maximum voltage output, denoted as VL,max, is calculated as

$$V_{L,max}^{Asym} = \frac{(N_{Lev}-1)}{2} \quad (6)$$

The 23 levels of output voltage that the proposed design generates range from zero to negative eleven volts, positive five volts to eleven volts, and negative eleven volts. Both the positive and negative levels of the 23-level MLI switching states are shown in TABLE 1. An essential quality is the total maximum blocking voltage, which is the sum of the maximum voltage stresses on all the switches added together algebraically. Here is how the MBV of certain switches is determined:

$$MBV_{S1} = MBV_{S2} = MBV_{S3} = V_a = 1V_{dc}$$
$$MBV_{S7} = MBV_{S9} = V_b = 3V_{dc}$$
$$MBV_{S5} = MBV_{S10} = V_c = 7V_{dc}$$
$$|MBV_{S4} = \frac{1}{2}(V_c + V_a) = 4V_{dc}$$
$$MBV_{S6} = MBV_{S11} = MBV_{S8} = MBV_{S12} = \frac{1}{2}(V_c + V_b) = 5V_{dc}$$

Simply put, TSV is the algebraic total of MBV across all switches, and it's expressed as exp.

$$TSV = MBV_{S1} + MBV_{S2} + MBV_{S3} \pm - - + MBV_{Sn} \quad (7)$$

$$TSV_{PU} = \frac{TSV}{V_{L.max}} \quad (8)$$

The computed value of $TSV^{Prop}$ for the suggested topology is

$$TSV^{Prop} = 4[5V_{dc}] + 2[3V_{dc}] + 2[7V_{dc}] + 3[V_{dc}] + 4V_{dc} \quad (9)$$

$$TSV^{Prop} = 47V_{dc}$$

$$TSV_{PU}^{Prop} = \frac{47V_{dc}}{11V_{dc}} = 4.27 \quad (10)$$

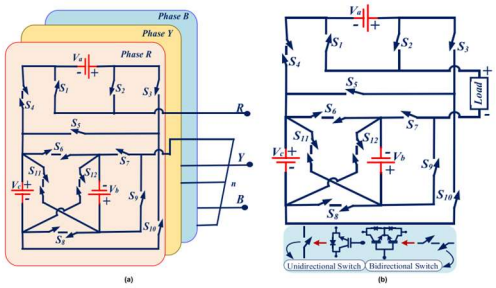


**Fig.3**. MLI topology with twenty-three levels (a) (b) three-phase + one-phase setup.

**Table 2.** Switching conditions of the proposed the MLI

| Positive level | | | | | | | | | | | | Output voltage (volts) | Negative levels | | | | | | | | | | | |
|---|---|---|---|---|---|---|---|---|---|---|---|---|---|---|---|---|---|---|---|---|---|---|---|---|
| $S_1$ | $S_2$ | $S_3$ | $S_4$ | $S_5$ | $S_6$ | $S_7$ | $S_8$ | $S_9$ | $S_{10}$ | $S_{11}$ | $S_{12}$ | | $S_1$ | $S_2$ | $S_3$ | $S_4$ | $S_5$ | $S_6$ | $S_7$ | $S_8$ | $S_9$ | $S_{10}$ | $S_{11}$ | $S_{12}$ |
| 0 | 1 | 0 | 1 | 0 | 0 | 1 | 1 | 0 | 0 | 0 | 0 | $11V_{dc}$ | 1 | 0 | 1 | 0 | 0 | 1 | 0 | 0 | 1 | 1 | 0 | 0 |
| 1 | 0 | 0 | 1 | 0 | 0 | 1 | 1 | 0 | 0 | 0 | 0 | $10V_{dc}$ | 0 | 1 | 1 | 0 | 0 | 1 | 0 | 0 | 1 | 1 | 0 | 0 |
| 1 | 0 | 1 | 0 | 1 | 0 | 1 | 1 | 0 | 0 | 0 | 0 | $9V_{dc}$ | 1 | 0 | 1 | 0 | 1 | 0 | 1 | 1 | 0 | 0 | 0 | 0 |
| 0 | 1 | 0 | 1 | 0 | 0 | 0 | 1 | 1 | 0 | 0 | 0 | $8V_{dc}$ | 1 | 0 | 1 | 0 | 0 | 1 | 1 | 0 | 0 | 1 | 0 | 0 |
| 1 | 0 | 0 | 1 | 0 | 0 | 0 | 1 | 1 | 0 | 0 | 0 | $7V_{dc}$ | 0 | 1 | 1 | 0 | 0 | 1 | 1 | 0 | 0 | 1 | 0 | 0 |
| 1 | 0 | 1 | 0 | 1 | 0 | 0 | 1 | 1 | 0 | 0 | 0 | $6V_{dc}$ | 1 | 0 | 1 | 0 | 1 | 0 | 0 | 1 | 1 | 0 | 0 | 0 |
| 0 | 1 | 0 | 1 | 0 | 0 | 0 | 0 | 1 | 0 | 0 | 1 | $5V_{dc}$ | 1 | 0 | 1 | 0 | 0 | 0 | 1 | 0 | 0 | 1 | 1 | 0 |
| 0 | 1 | 0 | 1 | 0 | 0 | 1 | 0 | 0 | 0 | 1 | 0 | $4V_{dc}$ | 1 | 0 | 1 | 0 | 1 | 1 | 0 | 0 | 1 | 0 | 0 | 0 |
| 1 | 0 | 0 | 1 | 0 | 0 | 1 | 0 | 0 | 0 | 1 | 0 | $3V_{dc}$ | 1 | 0 | 0 | 1 | 0 | 1 | 0 | 0 | 1 | 0 | 0 | 0 |
| 1 | 0 | 1 | 0 | 1 | 0 | 1 | 0 | 0 | 0 | 1 | 0 | $2V_{dc}$ | 0 | 1 | 0 | 1 | 0 | 1 | 0 | 0 | 1 | 0 | 0 | 0 |
| 0 | 1 | 0 | 1 | 0 | 1 | 1 | 0 | 0 | 0 | 0 | 0 | $1V_{dc}$ | 1 | 0 | 1 | 0 | 0 | 0 | 0 | 1 | 1 | 1 | 0 | 0 |
| 1 | 0 | 0 | 1 | 0 | 1 | 1 | 0 | 0 | 0 | 0 | 0 | $0V_{dc}$ | 1 | 0 | 0 | 1 | 0 | 1 | 1 | 0 | 0 | 0 | 0 | 0 |

Consequently, the suggested MLI architecture maximizes the use of DC sources with minimal TSV and switches, leading to a decrease in both volume and price. Table 2 displays the current flow to the load, MBV, voltage stress on the switches, and other relevant data. Redundant switches are a part of certain operational voltage levels. The suggested 23-level MLI topology is assessed for its merits and capabilities by comparing it with other contemporary topologies. Table 3 considers factors including cost, minimum number of conducting devices per level, total system voltage and current (TSVPU), DC sources, switches, component count factor (CCF), and driver circuit requirements.[31].

## 4 Analysis of Boost Converters for Solar Pv

Because temperature, irradiance, and the number of strings in parallel and series govern the PV array's current and voltage, selecting the right PV panel is critical. The chosen panel is the Trina Solar TSM-200

DC/DA01A, which has three strings of two series modules and three parallel modules. A perfect substitute model that o

| Levels | Current conducting path | Active sources | Stress on switches | Maximum Stress across switches | | Output Voltage (Volts) |
|---|---|---|---|---|---|---|
| $L_1$ | $V_C - S_4 - V_a - S_2 - L - S_7 - V_b - S_8 - V_c$ | $V_c + V_a + V_b$ | $S_1, S_6, S_9, S_{11}, S_{12}$ | $S_6$=$S_{11}$=$S_{12}$ | $5V_{dc}$ | $+11V_{dc}$ |
| $L_2$ | $V_C - S_4 - S_1 - L - S_7 - V_b - S_8 - V_c$ | $V_c + V_b$ | $S_6, S_9, S_{11}, S_{12}$ | $S_6$=$S_{11}$=$S_{12}$ | $5V_{dc}$ | $+10V_{dc}$ |
| $L_3$ | $V_C - S_5 - S_3 - V_a - S_1 - L - S_7 - V_b - S_8 - V_c$ | $V_c + V_b - V_a$ | $S_2, S_4, S_6, S_9, S_{10}, S_{11}, S_{12}$ | $S_{10}$ | $7V_{dc}$ | $+9V_{dc}$ |
| $L_4$ | $V_C - S_4 - V_a - S_2 - L - S_9 - S_8 - V_c$ | $V_c + V_a$ | $S_1, S_{11}$ | $S_{11}$ | $5V_{dc}$ | $+8V_{dc}$ |
| $L_5$ | $V_C - S_4 - S_1 - L - S_9 - S_8 - V_c$ | $V_c$ | $S_{11}$ | $S_{11}$ | $5V_{dc}$ | $+7V_{dc}$ |
| $L_6$ | $V_C - S_5 - S_3 - V_a - S_1 - L - S_9 - S_8 - V_c$ | $V_c - V_a$ | $S_2, S_4$ , $S_{10}, S_{11}, S_{12}$ | $S_{11}$=$S_{12}$ | $5V_{dc}$ | $+6V_{dc}$ |
| $L_7$ | $V_C - S_4 - V_a - S_2 - L - S_9 - V_b - S_{12} - V_c$ | $V_c - V_b + V_a$ | $S_1, S_6, S_7, S_8, S_{11}$ | $S_6$=$S_8$=$S_{11}$ | $5V_{dc}$ | $+5V_{dc}$ |
| $L_8$ | $V_b - S_{11} - S_4 - V_a - S_2 - L - S_7 - V_b$ | $V_a + V_b$ | $S_1, S_6, S_9$ | $S_9$ | $3V_{dc}$ | $+4V_{dc}$ |
| $L_9$ | $V_b - S_{11} - S_4 - S_1 - L - S_7 - V_b$ | $V_b$ | $S_6, S_9,$ | $S_6$=$S_9$ | $3V_{dc}$ | $+3V_{dc}$ |
| $L_{10}$ | $V_b - S_{11} - S_5 - S_3 - V_a - S_1 - L - S_7 - V_b$ | $V_b - V_a$ | $S_2, S_4, S_6, S_9$ | $S_9$ | $3V_{dc}$ | $+2V_{dc}$ |
| $L_{11}$ | $V_a - S_2 - L - S_7 - S_6 - S_4 - V_a$ | $V_a$ | $S_1$ | $S_1$ | $1V_{dc}$ | $+1V_{dc}$ |
| $L_{12}$ | $L - S_7 - S_6 - S_4 - S_1 - L - S_7$ | - | - | - | 0 | 0 |
| $L_{13}$ | $V_a - S_3 - S_{10} - S_8 - S_9 - L - S_1 - V_a$ | $-(V_a)$ | $S_2$ | $S_2$ | $1V_{dc}$ | $-1V_{dc}$ |
| $L_{14}$ | $V_b - S_9 - L - S_2 - V_a - S_4 - S_6 - V_b$ | $-(V_b - V_a)$ | $S_1, S_7$ | $S_7$ | $3V_{dc}$ | $-2V_{dc}$ |
| $L_{15}$ | $V_b - S_9 - L - S_1 - S_4 - S_6 - V_b$ | $-(V_b)$ | $S_7$ | $S_7$ | $3V_{dc}$ | $-3V_{dc}$ |
| $L_{16}$ | $V_b - S_9 - L - S_1 - V_a - S_3 - S_5 - S_6 - V_b$ | $-(V_b + V_a)$ | $S_2, S_4, S_7$ | $S_4$ | $4V_{dc}$ | $-4V_{dc}$ |
| $L_{17}$ | $V_c - S_{11} - V_b - S_7 - L - S_1 - V_a - S_3 - S_{10} - V_c$ | $-(V_c - V_b + V_a)$ | $S_2, S_4, S_5, S_9, S_{10}, S_{11}, S_{12}$ | $S_5$ | $7V_{dc}$ | $-5V_{dc}$ |
| $L_{18}$ | $V_a - S_3 - S_5 - V_c - S_8 - S_9 - L - S_1 - V_a$ | $-(V_c - V_a)$ | $S_2, S_4$ , $S_{10}$ | $S_{10}$ | $7V_{dc}$ | $-6V_{dc}$ |
| $L_{19}$ | $V_c - S_6 - S_7 - L - S_2 - S_3 - S_{10} - V_c$ | $-(V_c)$ | $S_5, S_{12}$ | $S_5$ | $7V_{dc}$ | $-7V_{dc}$ |
| $L_{20}$ | $V_c - S_6 - S_7 - L - S_1 - V_a - S_3 - S_{10} - V_c$ | $-(V_c + V_a)$ | $S_2$,$S_4$,$S_5$,$S_{12}$ | $S_5$ | $7V_{dc}$ | $-8V_{dc}$ |
| $L_{21}$ | $V_a - S_3 - S_5 - V_c - S_8 - V_b - S_7 - L - S_1 - V_a$ | $-(V_c - V_a + V_b)$ | $S_2, S_4, S_6, S_9, S_{10}, S_{11}, S_{12}$ | $S_{10}$ | $7V_{dc}$ | $-9V_{dc}$ |
| $L_{22}$ | $V_c - S_6 - V_b - S_9 - L - S_2 - S_3 - S_{10} - V_c$ | $-(V_a + V_b)$ | $S_5, S_7, S_8, S_{11}, S_{12}$ | $S_5$ | $7V_{dc}$ | $-10V_{dc}$ |
| $L_{23}$ | $V_c - S_6 - V_b - S_9 - L - S_1 - V_a - S_3 - S_{10} - V_c$ | $-(V_c + V_b + V_a)$ | $S_2, S_4, S_5, S_7, S_8$,$S_{11}, S_{12}$ | $S_5$ | $7V_{dc}$ | $-11V_{dc}$ |

**Table 3.** Comparisons of the proposed 23-level MLI with recent topologies.

| | *Quantitative analysis* | | | | | | *Qualitative analysis* | | | | |
|---|---|---|---|---|---|---|---|---|---|---|---|
| *Ref* | $N_{lev}$ | $N_{DC}$ | $N_{SW}$ | $N_{GDK}$ | $MCD$ | $N_{Var}$ | $CCF$ | $\%THD$ | $TSV_{PU}$ | $CF/N_{lev}$ | |
| | | | | | | | | | | $\alpha = 0.5$ | $\alpha = 1.5$ |
| [12] | 23 | 6 | 12 | 12 | 6 | 0 | 1.30 | 2.59 | 5.81 | 1.43 | 1.68 |
| [13] | 23 | 5 | 10 | 10 | 4 | 2 | 1.17 | - | 6.09 | 1.39 | 1.65 |
| [14] | 23 | 5 | 14 | 14 | 7 | 0 | 1.43 | 5.47 | - | - | - |
| [15] | 23 | 5 | 12 | 9 | 3 | 5 | 1.34 | 4.17 | - | - | - |
| [16] | 23 | 5 | 12 | 12 | 4 | 0 | 1.26 | 3.6 | 4.4 | 1.35 | 1.54 |
| [17] | 23 | 5 | 12 | 12 | 5 | 0 | 1.17 | - | 5.27 | 1.28 | 1.52 |
| Proposed | 23 | 5 | 12 | 12 | 7 | 0 | 1.17 | 3.23 | 4.27 | 1.27 | 1.45 |

As seen in Figure 4, solar PV works. Here, D stands for the diode, while RP and RS are the resistances of the cells that are linked in series and parallel, respectively. A perfect photovoltaic circuit would have a diode current of

$$i_d = I_0(e^{\frac{V_D}{\gamma V_T}} - 1) \quad (11)$$

The parameters that determine the thermal voltage VT = ( kT c q ), saturation current Io, and the ideality constant γ are the electron charge q, the cell temperature Tc, and Boltzmann's constant k.

Output power $P_{PV} = V_{PV} * I_{PV}$ (12)

Output current is

$$I_{PV} = I_S - I_d - I_p = I_s - I_0\left(e^{\frac{V_D}{\gamma V_T}} - 1\right) - I_p \quad (13)$$

$$I_{PV} = n_P I_S - n_P\left(e^{\left(\frac{V_D}{\gamma V_T}\right)\left(\frac{V_{PV}}{n_S} + \frac{R_S I_{PV}}{n_P}\right)} - 1\right) - \frac{n_P}{R_P}\left(\frac{V_{PV}}{n_S} + \frac{R_S I_{PV}}{n_P}\right) \quad (14)$$

Short circuit current IS

$$I_{S(T)} = I_{S(TR)}[\beta(T - T_R) + 1] \quad (15)$$

The PV datasheets display the H temperature coefficient values, TR reference temperature, and IS(TR) associated short circuit current.

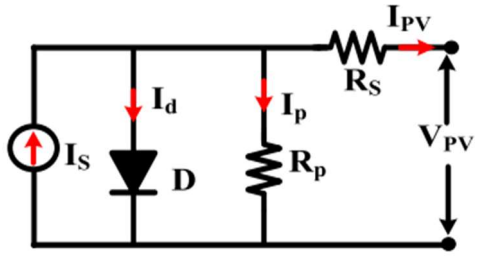


**Fig.4.** Model that is similar to Solar PV.

**Table 4.** Specifications of PV boost converter.

| 200W PV Module | | Boost Converter | |
|---|---|---|---|
| $P_{PV}$ | 200W | L | 1.28mH |
| $I_{PV}$ | 5.32A | C | 1.31$\mu$F |
| $V_{PV}$ | 37.6V | $V_{in} = V_{PV}$ | 112.8V |
| $I_{SC}$ | 5.60A | $\alpha$ | 0.718 |
| $V_{OC}$ | 46.0V | $V_{DC}$ | 400V |

Taking the irradiation level into account,

$$I_{S(G)} = I_{S(G_n)} \frac{G}{G_n} \quad (16)$$

The standard irradiation value is Gn. Once the saturation voltage (IPV) is zero, the current (I0) at time constant (TR) is determined by

$$I_0 = \frac{I_s}{\left(e^{\frac{V_D}{\gamma V_T}-1}\right)} \quad (17)$$

The primary problem in generating electricity from renewable sources is the low voltage output. The output of the RES is fed into a DC-DC boost converter, which then raises the voltage. The boost converter's output voltage is controlled by the control switch's duty cycle. By adjusting the switch ON time, the output voltage may be changed. The average output voltage over the duty cycle 'α' may be calculated using the following formula:

$$V_{dc} = V_{PV}\left(\frac{1}{1-\alpha}\right) \quad (18)$$

A capacitor's and inductor's values are determined by

$$L = \frac{V_{PV}\alpha}{(f_s * \Delta I_L)} \quad (19)$$

$$C = \frac{I_0\alpha}{(f_s * \Delta V_{dc})} \quad (20)$$

There is a ripple factor of 1IL for the input current and 1Vdc for the output voltage, and fs is the switching frequency. Limiting 1IL to 30% and generally assuming 1Vdc at 5% allows for more realistic inductor and capacitor value estimations. Listed in TABLE 4 are the characteristics of the solar PV jumper.

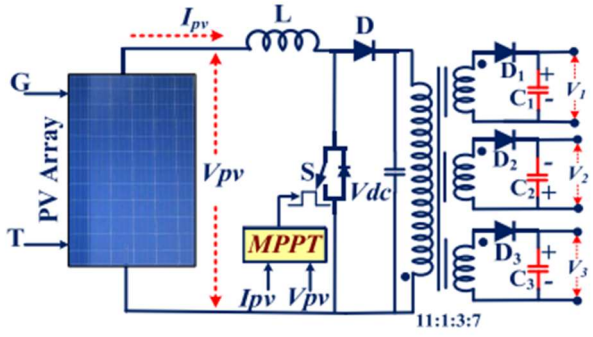


**Fig.5.** SIMO isolated DC-DC converter

The output of the DC-DC boost converter is received by a single-input multi-output (SIMO) circuit, as shown in Figure 5 [38]. Three output ports with a tur's ratio of 11:1:3:7 are supplied by the secondary winding of a multi-winding transformer upon receiving its input from a boost converter. A diode and capacitor are attached to the output terminal of each DC-DC converter. The diode is positioned so that reverse current cannot pass from the capacitor into the transformer windings. To manage the functioning of the boost converter, the maximum power point tracking (MPPT) controller takes temperature, solar radiation, DC link voltage, and the characteristics of the PV array ($V_{oc}$ and $I_{sc}$) as inputs. When irradiance circumstances are changing rapidly and the operating point oscillates around the MPP, the operational performance of traditional incremental and conductance MPPT algorithms is poor. An improved INC MPPT addresses these concerns [39]. The PV-fed MLI-DVR that is linked to the grid is shown schematically in Figure 6.

## 5 Operation and Control of Pv-Fed Mli-Dv with Fuzzy Logic

Depending on the load and voltage sag type, the DVR adjustment technique could differ. The rationale for this is because changes in voltage magnitude alone may influence certain loads, while changes in phase angle and both can affect others. Therefore, the control strategy to choose is determined by the load characteristics. It is possible to adjust for the voltage sag's magnitude and phase angle using the pre-sag compensation (PSC) method [40]. Because it keeps the load voltage constant in magnitude and phase angle relative to the pre-sag voltage, this approach is known as the voltage quality optimized technique. Consequently, the load is oblivious to any voltage irregularity. Figure displays the PSC vector representation. Adding additional actual power to the DVR during sag controls it, which changes the rating of the energy stored in direct current or received from the grid, and therefore increases the need for active power, apart from the reactive power injected by the inverter. No matter whether the sensitive loads are balanced or imbalanced, heaving phase jumps are permissible.

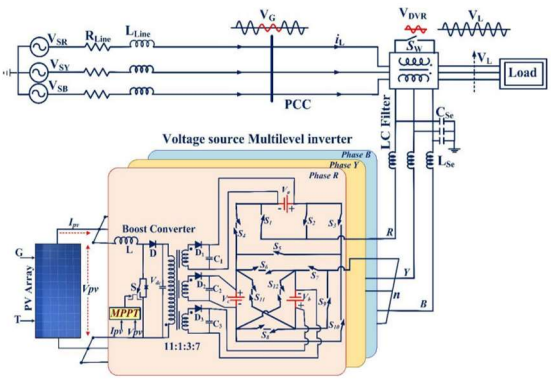


**Fig.6.**Proposed solar PV-fed MLI-DVR configuration.

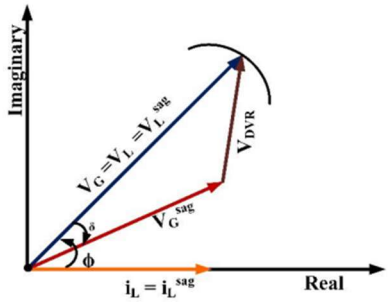


**Fig.7.** Pre sag voltage injection technique for DVR

The magnitude of VDVR may be found from equation 21, and the phase angle of VDVR can be calculated from equation 22.

$$V_{DVR.p} = \sqrt{2}\sqrt{(V_L)^2 + (V_G^{Sag})^2 - (2V_L V_{G.p}^{Sag}\cos(\delta_p))} \quad (21)$$

$$V_{DVR.p} = \tan^{-1}\left(\frac{V_L \sin\emptyset - V_{G.p}^{Sag}\sin(\emptyset-\delta_p)}{V_L\cos\emptyset - V_{G.p}^{Sag}\cos(\emptyset-\delta_p)}\right) \quad (22)$$

In this context, "VDVR" refers to the voltage that the DVR injects, "V Sag G" means the grid voltage at sag, "δ" means the angle that corresponds to the phase jump to V Sag G, and "p" means the phase that corresponds to the supply voltage, which might be R, Y, or B.

## 6 Control Scheme of the DV

The length (beginning and ending) and depth (phase jump) of a voltage disturbance are type-dependent. In [41], a number of techniques for detecting voltage fluctuations are detailed. In order to get the vectorized dq0 voltage components, we use the Park transformation on the three-phase load voltages VL RYB and the reference voltages Vref,RYB. The formula for the three-phase reference voltage is as follows:

$$\begin{bmatrix} V_{R\,ref} \\ V_{Y\,ref} \\ V_{B\,ref} \end{bmatrix} = V_{L\,max}\begin{bmatrix} \sin\omega t \\ \sin(\omega t - 120^0) \\ \sin(\omega t + 120^0) \end{bmatrix} \quad (23)$$

Then, as can be shown at the bottom of the following page, it passes through the Park transformation to transition from RYB to dq0 components (24). Examining the voltage's magnitude and phase shift after the load and reference voltages reach the dq0 frame will help you locate the error signal. Pictured in figure 8b is this.

$$|e_{rdq0}| = \sqrt{(V_{dref} - V_{di})^2 + (V_{qref} - V_{qi})^2 + (V_{0ref} - V_{0i})^2} \quad (24)$$

Choosing the Input and Output Variables for a Fuzzy Logic Controller

Power quality is impacted by the following critical variables:

- The voltage error, denoted as Ve, is the discrepancy between the reference voltage and the voltage that is actually output.
- The voltage error's rate of change, denoted as ΔVe.

The main result is:

Modulation Index (MI): Modulates the inverter's output amplitude to keep voltage levels where they should be.

### 6.1 Fuzzification

The membership functions are used to convert the input variables (Ve and ΔVe) and the output variable (MI) into phrases that are meaningful in language. Take this example:

**Ve**: Negative Large (NL), Negative Medium (NM), Negative Small (NS), Zero (Z), Positive Small (PS), Positive Medium (PM), Positive Large (PL).

**ΔVe**: Negative (N), Zero (Z), Positive (P).

**MI**: Decrease Large (DL), Decrease Small (DS), No Change (NC), Increase Small (IS), Increase Large (IL).

Rule Base

The input criteria are linked to the appropriate output action by means of an if-then rule set. Take this example:

If **Ve** is **PL** and **ΔVe** is **P**, then **MI** is **IL**.

If **Ve** is **Z** and **ΔVe** is **Z**, then **MI** is **NC**.

If **Ve** is **NM** and **ΔVe** is **N**, then **MI** is **DS**.

Inference Mechanism

A fuzzy output set is aggregated after the Mamdani inference technique has evaluated and combined the fuzzy rules.

Defuzzification

By using the centroid approach, the combined fuzzy output set may be transformed into a precise modulation index value.

When the voltage's magnitude and phase shift vary, the dq0 components will also change. Alterations to the

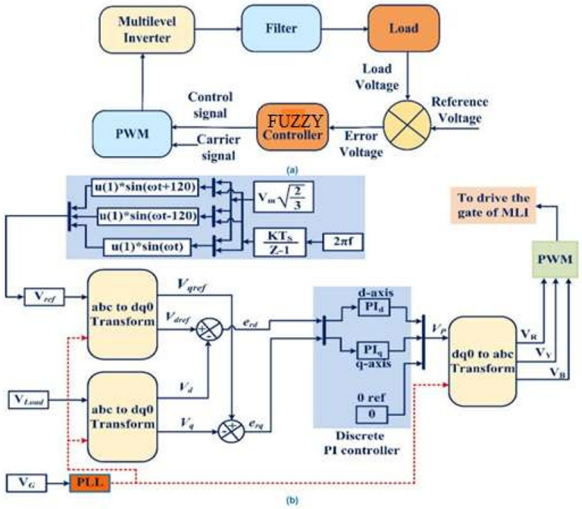


**Fig.8.** DVR WITH FUZZY controller

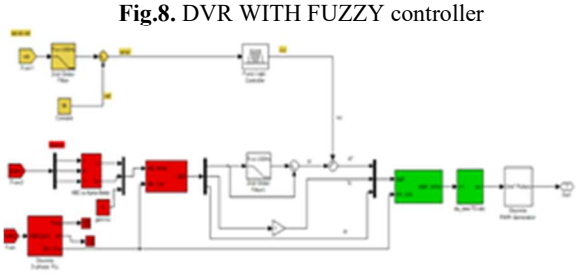

**Fig.9.** Simulation diagram of the proposed system

## 7 Simulation Results

Simulations in software like MATLAB/Simulink verify the FLC. Modelling the photovoltaic array, direct current to direct current converter, multilevel inverter, and grid interface is part of the setup. The effectiveness of the FLC in preserving power quality under diverse circumstances is assessed by a battery of tests. After the simulation runs well, the FLC is translated into hardware and tested with a real PV system and a multilevel inverter. The system's reaction to fluctuations in solar irradiance, load, and grid conditions are observed.

Our evaluation of the suggested multilayer inverter solar PV supplied DVR is based on its ability to improve the voltage profile. The MATLAB/Simulink platform is used to display the findings. You may find the DVR parameters in Table 2. A 10-kilowatt (1:1) injection transformer with 400 volts connects the DVR to the system. A boost converter may raise a PV array's output voltage to 400V. An 8 kW, 0.85 lagging PF linear load (RL Load) and a 500Ah battery with a typical 400V voltage are taken into account in order to maintain a constant DC link voltage. The results of the EINC MPPT-based combined PV and boost converter modelling are shown in Figure. 10. at MPP, PV produces

**Table 5.** DVR parameters and ratings

| | |
|---|---|
| Source (AC grid) | 400V, 50Hz |
| DC-Link voltage | 400V |
| Filter | L=50mH, c=80μF, R=1.5Ω |
| Switching Frequency | 5kHz |
| Transformer ratio | 1:1 |

112.8% of the voltage is transformed into 400 volts at the DC connection using a boost converter. An asymmetrical 23-level MLI's R phase voltage waveform is shown in Figure 11. In order to generate voltage sag mode, overload is applied at intervals between 0.2 and 0.285 seconds. The load point reference voltage is compared to a 0.5pu sag in this test.

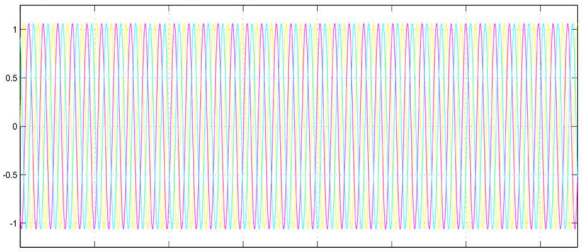

**Fig.10.** Grid Voltage

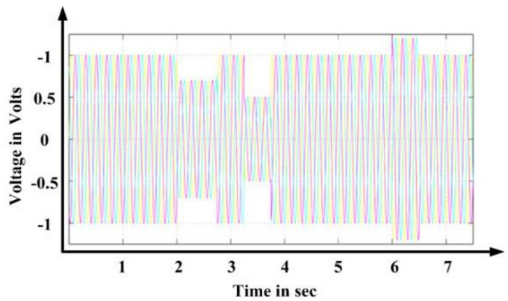


**Fig.11.** Source Voltage

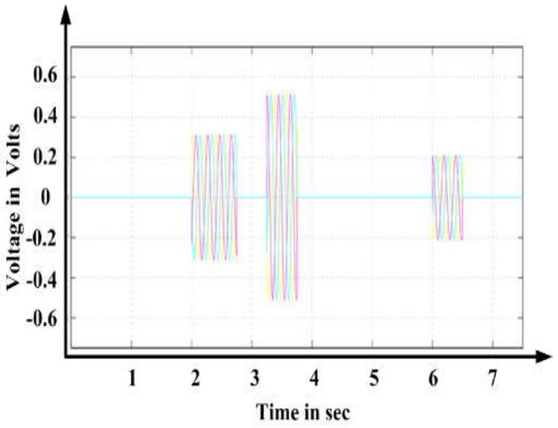


**Fig.12.** DVR Voltage

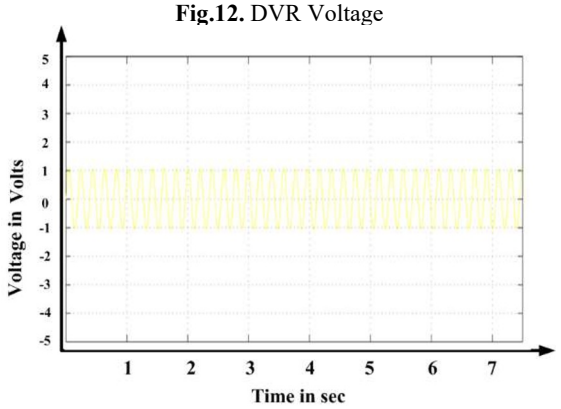


**Fig.13.** Single phase Grid Voltage

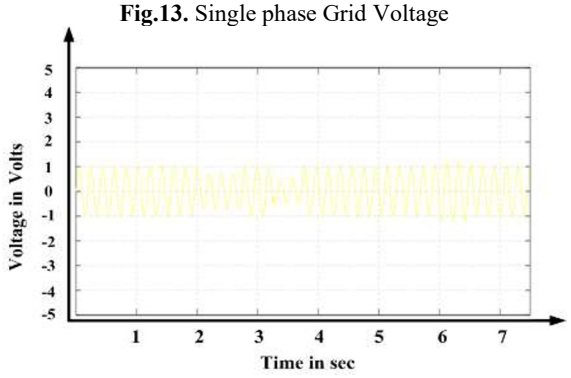


**Fig. 14.** Single phase Source Voltage

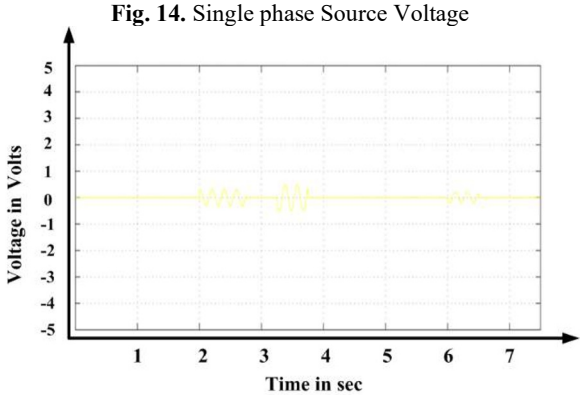


**Fig.15.** DVR Voltage

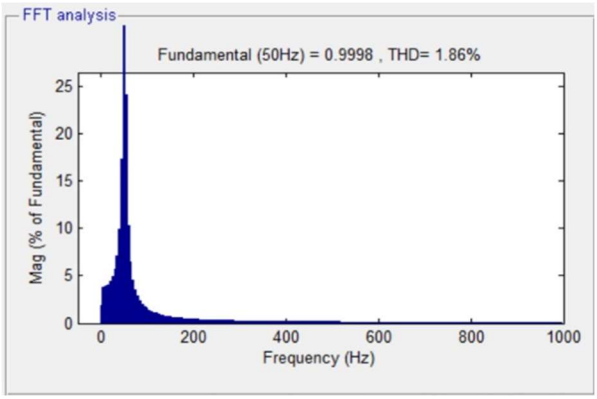


**Fig.16.** THD % using Fuzzy Controller

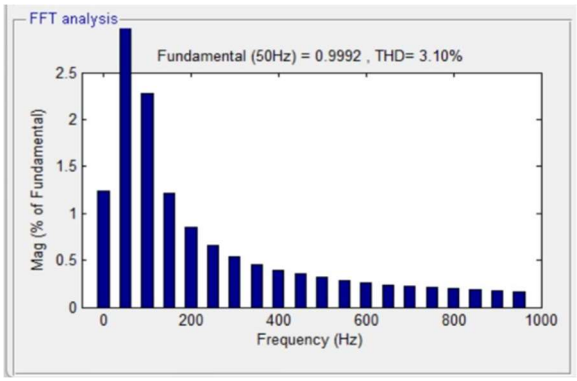


**Fig.17**. THD % using PI Controller

**Table. 6** Comparison of %THD

| Sl. No | PI Controller THD % | Fuzzy Controller THD % |
|---|---|---|
| 1 | 3.10 | 1.86 |

## 8 Conclusion

A synthesized output voltage of the proposed MLI is obtained with a low THD utilizing fewer circuit components. The results of the proposed PV-fed MLI-DVR are verified with the fuzzy logic controller simulator testing platform. The proposed system efficiently minimizes the voltage sag and preserves the DC link voltage to be stable. The fuzzy logic controller for a multilevel inverter in a grid-connected solar PV system enhances power quality by reducing voltage fluctuations, harmonic distortion, and reactive power imbalances. The maximum power can be extracted from the PV modules using INC MPPT technique. The adaptive nature of fuzzy logic control makes it well-suited for the dynamic and nonlinear characteristics of renewable energy systems.

## References

1. Reddy, S. V. R., Premila, T. R., Reddy, C. R., & Reddy, B. N. (2023). Zero power mismatch islanding detection algorithm for hybrid distributed generating system. Transactions on Energy Systems and Engineering Applications, 4(2), 1-12.
2. D. Li, T. Wang, W. Pan, X. Ding, and J. Gong, ‘‘A comprehensive review of improving power quality using active power filters,’’ Electr. Power Syst. Res., vol. 199, Jun. 2021, Art. no. 107389, doi: 10.1016/j.epsr.2021.107389.
3. R. Sepehrzad, A. Mahmoodi, S. Y. Ghalebi, A. R. Moridi, and A. R. Seifi, ‘‘Intelligent hierarchical energy and power management to control the voltage and frequency of micro-grids based on power uncertainties and communication latency,’’ Electr. Power Syst. Res., vol. 202, Jan. 2022, Art. no. 107567, doi: 10.1016/j.epsr.2021.107567.
4. F. K. De Araújo Lima, J. M. Guerrero, F. L. Tofoli, C. G. C. Branco, and J. L. Dantas, ‘‘Fast and accurate voltage sag detection algorithm,’’ Int. J. Electr. Power Energy Syst., vol. 135, Feb. 2022, Art. no. 107516, doi: 10.1016/j.ijepes.2021.107516.
5. C. Dhanamjayulu and S. Meikandasivam, ‘‘Fuzzy controller-based design of 125 level asymmetric cascaded multilevel inverter for power quality improvement,’’ Anal. Integr. Circuits Signal Process., vol. 101, no. 3, pp. 533–542, 2019.
6. M. Bajaj, ‘‘Design and simulation of hybrid DG system fed single-phase dynamic voltage restorer for smart grid application,’’ Smart Sci., vol. 8, no. 1, pp. 24–38, Apr. 2020, doi: 10.1080/23080477.2020.1748928.
7. A. B. Kanase-Patil, A. P. Kaldate, S. D. Lokhande, H. Panchal, M. Suresh, and V. Priya, ‘‘A review of artificial intelligence-based optimization techniques for the sizing of integrated renewable energy systems in smart cities,’’ Environ. Technol. Rev., vol. 9, no. 1, pp. 111–136, Jan. 2020, doi: 10.1080/21622515.2020.1836035.
8. Priya, B. K., Reddy, D. A., Soliman, W. G., Rani, A. D., Kalahasthi, N., & Reddy, D. R. K. (2022). Hybrid stepper motor: Model, open-loop test, traditional PI, optimized PI, and optimized gain scheduled PI controllers. International Journal of Control, Automation and Systems, 20(12), 3915-3922.
9. Bhanutej, J. N., Kumar, G. G., Kalahasthi, N., & Mahalakshmi, K. S. (2023, December). Analysis and Design of Reliable Converter Topology for Grid Connected PV Systems with ANN Controller. In 2023 3rd International Conference on Smart Generation Computing, Communication and Networking (SMART GENCON) (pp. 1-5). IEEE.
10. Kalyan, C. N. S., Goud, B. S., Reddy, C. R., Reddy, B. N., Bajaj, M., & Sudhakar, A. V. (2021, September). Falcon optimizer based PIDD controller for AGC of dual area realistic system with AC-DC links. In 2021 International Conference on Technology and Policy in Energy and Electric Power (ICT-PEP) (pp. 6-10). IEEE.
11. Goud, B. S., Reddy, C. R., Rakesh, T., Rajesh, N., Reddy, B. N., & Aymen, F. (2021). Grid integration of renewable energy sources using GA technique for improving power quality. International Journal

of Renewable Energy Research (IJRER), 11(3), 1390-1402.

12. Kalahasthi, N., Kanthi, S. C., Guntipally, N., Bongarapu, R. R., & Kopati, G. (2024, February). SU DO KU Configuration of Solar PV Array Under Partial Shading Condition. In 2024 3rd International conference on Power Electronics and IoT Applications in Renewable Energy and its Control (PARC) (pp. 481-486). IEEE.
13. Srilakshmi, Koganti, Sravanthy Gaddameedhi, Subba Reddy Borra, Praveen Kumar Balachandran, Ganesh Prasad Reddy, Aravindhababu Palanivelu, and Shitharth Selvarajan. "Optimal design of solar/wind/battery and EV fed UPQC for power quality and power flow management using enhanced most valuable player algorithm." Frontiers in Energy Research 11 (2024): 1342085.
14. E. Salary, M. R. Banaei, and A. Ajami, ‘‘Analysis of hybrid multilevel inverters using a reduced voltage stress switch,’’ Cankaya Univ. J. Sci. Eng., vol. 13, no. 2, pp. 51–56, 2016.
15. S. Galeshi and H. Iman-Eini, ‘‘Dynamic voltage restorer employing multilevel cascaded H-bridge inverter,’’ IET Power. Electron., vol. 9, no. 11, pp. 2196–2204, Sep. 2016, doi: 10.1049/iet-pel.2015.0335.
16. E. Salari and A. D. Falehi, ‘‘A novel 49-level asymmetrical modular multilevel inverter: Analysis, comparison and validation,’’ Anal. Integr. Circuits Signal Process., vol. 101, no. 3, pp. 611–622, Dec. 2019.
17. Ramadevi, Alapati, Koganti Srilakshmi, Praveen Kumar Balachandran, Ilhami Colak, C. Dhanamjayulu, and Baseem Khan. "Optimal Design and Performance Investigation of Artificial Neural Network Controller for Solar-and Battery-Connected Unified Power Quality Conditioner." International Journal of Energy Research 2023, no. 1 (2023): 3355124.
18. R. J. Satputaley and V. B. Borghate, ‘‘Performance analysis of DVR ‘using new reduced component’ multilevel inverter,’’ Int. Trans. Electr. Energy Syst., vol. 27, no. 4, pp. 1–11, 2017, doi: 10.1002/etep.2288.